Supporting Information to

Effects of Architecture on the Stability of Thermosensitive Unimolecular Micelles

by

Alexander A. Steinschulte, Bjoern Schulte, Stephan Rütten, Thomas Eckert, Jun Okuda, Martin Möller, Stefanie Schneider, Oleg V. Borisov, Felix A. Plamper

EXPERIMENTAL SECTION

MATERIALS. Anhydrous tetrahydrofuran (THF; destabilized), pyrene, 4-(dicyanomethylene)-2-methyl-6-(*p*-dimethylaminostyryl)-4*H*-pyran (4HP), coumarin 153, poly(ethylene glycol) monomethyl ether (M_n = 5000 g/mol according to the manufacturer's data; $Đ_{M,SEC}$ = 1.1 and $M_{n,MALDI}$ = 4950 g/mol, $Đ_{M,MALDI}$ = 1.01; dried in vacuo after precipitation twice in anhydrous diethylether and then hexane respectively), poly(propylene glycol) monobutyl ether (M_n ≈ 2500 g/mol according to the manufacturer's data; $Đ_{M,SEC}$ ≈ 1.4), methanesulfonyl chloride, anhydrous tetrahydrofuran (THF; destabilized), bromoisobutyryl bromide and *N,N,N´,N´´,N´´´,N´´´*- hexamethyltriethyltriamine (HMTETA) was delivered by Sigma Aldrich. Sodium hydride (50% in paraffin oil), molecular sieves (4Å) and pH 8 buffer solution (20°C; 0.013 M sodium tetraborate / 0.021 M hydrochloric acid) were delivered by Fluka. Sodium chloride was obtained by KMF (Lohmar, Germany). Poly(propylene glycol) (M_n = 4000 g/mol according to the manufacturer's data; $Đ_{M,SEC}$ = 1.1 and $M_{n,MALDI}$ = 4170 g/mol, $Đ_{M,MALDI}$ = 1.01) was delivered by Polysciences, Warrington, PA, USA. *N,N*-dimethylaminoethyl methacrylate (DMAEMA; purified by filtration over basic alumina), silica and *N,N*-dimethyl-4-pyridinamine (DMAP) were purchased from Acros Organics, Geel, Belgium. Chloroform, *n*-hexane, 1,4-dioxane (HPLC-grade), ethyl acetate,

methanol, anhydrous diethylether and anisole were obtained by VWR. Triethylamine, butanol, n-heptanes and alumina were obtained from Merck (Darmstadt, Germany). CuCl and $CuCl_2$ were obtained from Alfa Aesar. Acetone and THF for the preparation was bought by AppliChem (Darmstadt, Germany). Dichloromethane was bought from Promochem (Wesel, Germany). Basic alumina (Alumina B-Super 1) was obtained from MP Biomedicals (Enschede, Germany). Monomesylated poly(ethylene oxide) (M_n = 5000 g/mol; $Đ_{M,SEC}$ = 1.1) was prepared according to reference from above-mentioned poly(ethylene glycol) monomethyl ether.[1] Bismesylated poly(propylene oxide) (M_n = 4 kg/mol; $Đ_{M,SEC}$ = 1.1) was prepared according to reference.[2] Regenerated cellulose dialysis membranes (Cellu Sep H1, MWCO 3500; Cellu Sep T2, MWCO 12000) were purchased from Interchin. For reagents, the highest purities available were acquired and used as delivered (except where otherwise stated). The synthesis of the star polymers PEO_{114}-$(PDMAEMA_{90})_{3.1}$-PPO_{69} and PEO_{114}-$(PDMAEMA_{110})_{2.5}$ is described in references (the indexes account for the number-average degree of polymerization per block and the arm number respectively).[2, 3] The synthesis of the diblock copolymer PPO_{69}-*b*-$PDMAEMA_{100}$ is described below.

SYNTHESIS.

Poly(ethylene oxide)-block-poly(propylene oxide) (PEO_{114}-PPO_{69})

The bismesylated poly(propylene oxide) (2.1 g, $5.25 \cdot 10^{-4}$ mol) was dissolved in 5 mL dry, inhibitor-free THF and heated at 75°C. A mixture of poly(ethylene glycol) (0.5 g, $1 \cdot 10^{-4}$ mol) and NaH (50 mg, 50% $1.04 \cdot 10^{-3}$ mol) in 10 mL dry THF was slowly added with a syringe under nitrogen counterflow and stirring before it was refluxed overnight at 75°C. The next day, 50 mg NaH and 10 mL THF were added under N_2-counterflow, stirring and reflux. After 6 h, the mixture was cooled down and further 10 mL THF were added. Then, the mixture was acidified by addition of acetic acid until wet pH paper shows neutral pH. The mixture was

centrifuged at 5000 rpm and the supernatant was concentrated. It was dissolved in 10 mL THF and precipitated in the freezer over night. The next day, heptane was added and the mixture was centrifuged (at 20°C; 5000 rpm). Again, the precipitate was dissolved in hot hexane, precipitated in the freezer and centrifuged at 5000 rpm in order to remove left-over PPO, which was not incorporated into the diblock. Then, the precipitate was dried in vacuo. The next day, it was dissolved in cold water and the polymer was freeze-dried to yield 0.36 g (40%) polymer. SEC (DMF, 1 g/L LiBr; PMMA calibration): M_n = 16900 g/mol, $Đ_M$ = 1.10; δ_H(400 MHz; $CDCl_3$; Me_4Si) 3.6 (s, PEO-*H*), 3.6-3.5 (m, O-CH_2-CHCH_3-O), 3.45-3.25 (m, O-CH_2-C*H*CH_3-O), 1.2-1.1 (m, O-CH_2-CHC*H*$_3$-O).

PPO-based macroinitiator PPO_{69}-Br[4, 5]

Poly(propylene glycol) monobutyl ether (3 g; $M_n \approx$ 2500 g/mol; $DP_n \approx$ 43; $1.2 \cdot 10^{-3}$ mol) was dissolved in triethylamine (2 g) and dichloromethane (10 g), before 10 grains of a molecular sieve was added and left for 2 h. Then, the grains were removed and the solution was cooled with ice (the flask was equipped with a $CaCl_2$ water trap). 2-Bromo-2-methylpropanoyl bromide (0.55 g, $2.4 \cdot 10^{-3}$ mol) was slowly added over a period of 15 min. Then, the mixture was left to warm up overnight under stirring. The next day, the mixture was refluxed for 2 h, before the mixture was left for stirring 2 more days. Then, the mixture was concentrated, redispersed in hexane, filtered over basic alumina and once more concentrated. The product was dialyzed against acetone (MWCO 1000, 3 d), which yields 200 mg of product after drying in vacuo. ^{1}H NMR shows 61 % esterification under the assumption $M_n \approx$ 2500 g/mol. However, dialysis apparently fractionated the sample, leaving pure macroinitiator of higher M_n inside the dialysis membrane ($M_n \approx$ 4000 g/mol when assuming full esterification of the telechelic polymer; both butyl and allyl – as made by transfer to monomer during anionic PO - polymerization – comprise the other endgroup; $DP_n \approx$ 69). SEC (DMF, 1

g/L LiBr; PMMA calibration): M_n = 3700 g/mol, $Đ_M$ = 1.63; δ_H(400 MHz; $CDCl_3$; Me_4Si): 5.89 (0.4H, m, H_2C=C*H*CH_2-O, endgroup made by transfer to monomer during anionic polymerization), 5.26 (0.4H, m, H*H*C=C*H*CH_2-O), 5.16 (0.4H, m, *H*HC=C*H*CH_2-O), 5.05 (1H, m, $(CH_3)_2$CBrC(=O)-C*H*(CH_3)-CH_2-O), 4.00 (1H, d, ?), 3.6-3.45 (140H, m, O-C*H*$_2$-CHCH_3-O), 3.45-3.3 (70H, m, O-CH_2-C*H*CH_3-O), 1.92, (6H, s, (C*H*$_3$)$_2$CBrC(=O)-), 1.66 (12H, s, ?), 1.53 (1.2H, m, CH_3C*H*$_2$C*H*$_2$$CH_2$-O, initiator moiety as endgroup), 1.36 (1.2H, m, CH_3C*H*$_2$C*H*$_2$$CH_2$-O, initiator moiety as endgroup), 1.3-1.2 (3H, m, $(CH_3)_2$CBrC(=O)-CH(C*H*$_3$)-CH_2-O), 1.2-1.0 (210H, m, O-CH_2-CHC*H*$_3$-O), 0.91 (1.7H, t, J = 7.2 Hz, C*H*$_3$$CH_2$$CH_2$$CH_2$-O, initiator moiety as endgroup).

PPO-*b*-PDMAEMA diblock copolymers (PPO_{69}-*b*-$PDMAEMA_{68}$) and (PPO_{69}-*b*-$PDMAEMA_{100}$)

The PPO-based macroinitiator (100 mg; 2.1 wt.% Br; $2.5 \cdot 10^{-5}$ mol), $CuCl_2$ (0.7 mg; $5 \cdot 10^{-6}$ mol) and CuCl (2.4 mg; $2.4 \cdot 10^{-5}$ mol) were mixed with anisol (1 mL; filtered over basic alumina), purged with nitrogen and heated to 80 °C under stirring. Then, a mixture of the ligand HMTETA (13.3 mg) and the monomer DMAEMA (1.16 g) was deoxygenated, as well. A part of this solution (in total 0.612 g; 0.605 g DMAEMA - $3.71 \cdot 10^{-3}$ mol; 6.9 mg HMTETA - $3 \cdot 10^{-5}$ mol) was introduced into the hot reaction mixture by use of a nitrogen-purged syringe. The polymerization was stopped for one part by removal of 0.75 mL of the reaction mixture with help of a syringe (under nitrogen counter-flow) and addition to chloroform (5 mL) after 105 min reaction time (the conversion was determined as 48 % by NMR). The other part of the polymerization mixture was terminated accordingly after 4 h (conversion: 70 % by NMR). Both products were purified by filtering over silica, concentrated and dialyzed against dioxane (MWCO 3500; 1 d). After freeze-drying, 0.175 g and 0.25 g of diblock copolymers were obtained respectively. SEC_1 (DMF, 1 g/L PMMA calibration): M_n = 10400 g/mol, $Đ_M$ = 1.35; SEC_2 (DMF, 1 g/L LiBr; PMMA calibration): M_n

= 21900 g/mol, $Đ_M$ = 1.10; δ_H(400 MHz; $CDCl_3$; Me_4Si): 4.2 - 3.9 (O-C*H*$_2$CH$_2$-N, PDMAEMA), 3.6-3.45 (m, O-C*H*$_2$-CHCH$_3$-O, PPO), 3.45-3.25 (m, O-CH$_2$-C*H*CH$_3$-O, PPO), 2.65-2.5 (O-CH$_2$C*H*$_2$-N, PDMAEMA), 2.35 - 2.25 (-N(C*H*$_3$)$_2$, PDMAEMA), 2.0 - 1.7 (PDMAEMA backbone C*H*$_2$); 1.17-1.1 (m, O-CH$_2$-CHC*H*$_3$-O, PPO), 1.1 – 0.85 (PDMAEMA backbone C*H*$_3$).

METHODS.

NMR. The NMR spectra were measured with a 400-MHz Bruker DRX 400 NMR spectrometer at 23 °C. Unless otherwise stated, $CDCl_3$ was used as solvent (usually 10 mg·mL^{-1}). The chemical shifts are presented in parts per million downfield from the TMS standard.

Combined dynamic light scattering (DLS) and static light scattering (SLS). As an example, the PEO$_{114}$-*block*-PPO$_{69}$ polymer samples were prepared in concentrations of 0.16 g·L^{-1} in buffered 0.1 M NaCl solution (pH 8). The solutions were filtrated after cooling to 5 °C over a regenerated cellulose membrane 0.45 µm (and analyzed as described below; see also Ref.[6]).

Similarly, the miktoarm terpolymer samples were prepared in concentration of 1 g·L^{-1} in buffered 0.1 M NaCl solution (pH 8) and filtrated at 5°C over a regenerated cellulose membrane 0.45 µm. The light scattering measurements were performed with an ALV 5000 E autocorrelator equipped with a red Laser (λ = 633 nm) with an average heating rate of ~ 6 K/h (taking ~ 13 h for measuring at several angles from 30° to 140° at every 4 K interval between 1°C and 73°C). The time-resolved signal of two Single Photon Counting Modules (SPCM-CD 2969; Perkin Elmer) was cross-correlated. The combined DLS / SLS treatment was adapted from references.[7, 8] Hereby, the CONTIN analysis was performed in an angular and temperature dependent way. For each measurement (sampling time 5 min), the intensity-

weighted decay-time τ distributions (as obtained from the field autocorrelation function obtained by use of the Siegert relation)[9] were analyzed in respect to multimodality, where for each diffusive mode its (intensity-)average decay rate Γ ($1/\tau$) was extracted (if necessary, the probability factor of the CONTIN algorithm was adjusted in order to increase resolution). Then, the decay rates were plotted against the squared length of the scattering vector q^2 for each temperature. The slope gave the diffusion coefficient D and its value was transformed to the hydrodynamic radius R_h by the Stokes Einstein equation.

Furthermore, the respective intensity for each diffusive mode was extracted by subdividing the overall count rate (solvent scattering was neglected, which results in an estimated error < 1% by comparison of the observed count rates). Therefore, the decomposed intensities for each species can be plotted against the squared length of the scattering vector q^2 and extrapolated toward $q^2 \rightarrow 0$. The extrapolated intensities, which are both correlated with the molar mass and the concentration of the species, are therefore plotted against the temperature in order to gain further information on the structural changes during a temperature scan. By using a scaling approach, the molar mass M of the scattering entities can be correlated to the hydrodynamic radius R_h. Here we used a Daoud and Cotton scaling for star-shaped entities (with variable arm number f or aggregation number N_{agg} and constant arm length; see also Ref.[6]).[10]

Fluorescence spectroscopy. The aqueous pyrene stock solution was prepared by addition of 2 µL of a 1 g/L pyrene solution in THF to 20 mL of a buffered 0.1 M NaCl solution (pH 8) in order to obtain a pyrene concentration of 10^{-4} g/L ($5 \cdot 10^{-7}$ M). We choose this preparation method after having assessed the influence of organic solvent traces on the phase-separation and fluorescence properties.[6] In a similar way, the 4-(dicyanomethylene)-2-methyl-6-(*p*-$^{6}10^{-6}$ M (e.g. by addition of ~ 0.5 µL of a 10 g/L 4HP THF solution to 20 mL of a pH 8 buffered 0.1 M NaCl solution). The solutions were equilibrated over night (in the refrigerator). For the

measurement of the dye's fluorescence in pure PPO polymer, a 10^{-6} mol/L solution of the dye was prepared (e.g. ~ 0.5 µL of a 1 g/L 4HP solution in acetone was added to 2 mL of pure PPO 4000). For measurements in pure PDMAEMA and PDMAEMA/PPO complexes, 0.5 g total polymer was dissolved in ~ 2 mL of dioxane, before ~ 1.5 µL of a 0.1 g/L 4HP solution in dioxane was added. Herefore, linear $PDMAEMA_{1200}$ was used (GPC data with PMMA calibration: M_n = 170 kg/mol, $Đ_M$ = 1.9), as synthesized in Ref.[6] The complex was prepared according to a PDMAEMA/PPO ratio, which is reported to give full miscibility (0.07 g PPO_{69}, purchased by Polysciences, and 0.43 g $PDMAEMA_{1200}$).[11] Then all PDMAEMA containing polymers were freeze-dried and tempered within a cuvette at 85°C for 1 day in order to get a rubbery chunk of polymer, suitable for temperature dependent fluorescence measurements.

Fluorescence spectra were recorded using a Jasco FP-6500 Spectrofluorometer using the following conditions: excitation at $\lambda_{excitation}$ = 333 nm and recording range $\lambda_{emission}$ =340-500 nm for measurements with pyrene (extraction of the intensity of the first and third vibronic band at 372 nm and 384 nm, respectively), excitation at $\lambda_{excitation}$ = 470 nm and recording range $\lambda_{emission}$ = 480-750 nm for 4HP (extraction of the wavelength at the emission maximum λ_{max}; total intensity extracted by integration over full range), 3 nm slit width for excitation and emission, resolution 0.5 nm. The spectrometer was equipped with a Jasco PCT-163T temperature controller. The sample was heated in 2 K intervals (heating rate 20 K/h; equilibration time 1 min before each measurement; average heating rate ~ 12 K/h).

Measurement of the "critical micellization concentration" cmc by steady state fluorescence spectroscopy: The aqueous pyrene stock solution was prepared by addition of 2 µL of a 1 g/L pyrene solution in ethanol into a glass vial, which was air-dried successively. Then, 20 mL of a buffered 0.1 M NaCl solution (pH 8) were added in order to obtain a pyrene concentration of $1 \cdot 10^{-4}$ g/L ($5 \cdot 10^{-7}$ M) after dissolution under shaking for 1 h. From this pyrene stock

solution, a polymer stock solution was prepared by dissolution of 1 mg of the respective polymer in 1 mL of the pyrene solution. Then, the polymer mixture was diluted with the pyrene stock solution to the respective concentrations (excitation at 320 nm and recording range 340-500 nm for measurements with pyrene). The solutions were equilibrated in the refrigerator overnight and approximately one hour at RT before each measurement. Prolonged equilibration (e.g. keeping the solutions for 2 h at 50 °C and then 1 h at RT) does not change the spectra (error in the range of 1 %). The ratio of the first and the third vibronic band of the pyrene's emission spectrum was used for the detection of hydrophobic environments, which surround the pyrene probe molecules.

Infrared (IR) spectroscopy. Temperature-dependent Fourier Transform IR-spectroscopy (FTIR) was performed by use of a Shimadzu IRPrestige-21 spectrometer (Shimadzu Corporation, Kyoto, Japan), equipped with a Peltier-based thermostatable cell holder (Pike Technologies, Madison, WI, USA). CaF_2 windows (Pike Technologies) were used with a Teflon spacer of 0.02 mm thickness. 256 spectra were recorded for background (pure solvent) and sample each, which were subtracted after data acquisition. As solvent, the usual aqueous salt solutions were replaced by transfer to D_2O in order to shift the absorption band of water and reduce its influence on the carbonyl band. This was accomplished by freeze drying of a pH 8 buffer solution, containing 0.1 M NaCl, and dissolution of the dry salt with an equivalent volume D_2O. Then, the polymer concentration was adjusted to 3 g/L (in order to resolve peaks, a higher polymer concentration was required compared to the standard 1 g/L). The IR-Solution software (Shimadzu) was used for background subtraction (solvent measured at the respective temperature), baseline correction and smoothing of the data.

Titration. 5.5 mg – 6 mg of polymer were dissolved in 5.5 mL of 0.1 M NaCl in order to keep the PDMAEMA concentration constant. The solution was titrated with 0.1 M HCl in 1 µL portions by a Methrohm 665 autotitrator (total added amount of HCl ~ 0.35 mL). The

titrations were performed at 25 °C. After heating the sample within a tempered titration cell to 60 °C, backtitrations were performed with 0.1 M NaOH. The starting point of backtitration and the endpoints was determined by the extremes in the derivative of the pH against volume of the titrant $V_{Titrant}$ (point of inflection), yielding a plot of pH against degree of neutralization α.

Scanning transmission electron microscopy (STEM) and **Scanning Electron Microscopy** (SEM). For cryogenic scanning transmission electron microscopy (cryo-STEM), one drop of sample was put on formvar/carbon-coated copper grid (S162-4, Plano, Wetzlar, Germany) and then shock-frozen in liquid methane. Afterwards, it was transferred into the cryo-holder and inserted into the microscope. For vitrification from 70°C, the polymer solution was heated to 70°C with 20 K/h and then left over night in the thermostat (Julabo). One drop of the hot sample was transferred with a preheated syringe onto the grid, which was immediately plotted with plotting paper in order to remove the majority of solution. Right after this, the grid was immersed into liquid methane (condensed by help of liquid nitrogen). The time of transfer of the drop and vitrification took approximately 2s. After transfer to the microscope, cryo-SEM images were taken (no freeze-fracture in this case). All images were recorded on an Ultra-High Resolution FE-SEM S-4800 operated at 30 kV.

Optical microscope. The miktoarm terpolymer (1 mg) was dissolved in 1 mL aqueous 0.1 M NaCl pH 8 buffer solution. The solution was preheated with 20 K/h to 70 °C using a thermostat. The pictures were obtained with a Leica DMLB microscope equipped with a Linkan css 450 thermostatable sample holder and Kappa camera. The lens was a Leica N PLAN H50x, 0.50.

Small Angle X-Ray Scattering (SAXS). SAXS measurements were performed with a S-Max3000 system with a MicroMax-002+ X-ray microfocus generator by Rigaku in a *q*-range

from 0.004–0.16 $Å^{-1}$ at 3, 20, 45 and 70 ° C (λ = 1.54 Å). The form factor was modeled and fitted by use of the program SASfit ver. 0.93.2, using the model "SPHERE+chains(RW)".

RESULTS AND DISCUSSION

PEO-b-PPO Diblock Synthesis. The reactivity of mesylated PPO towards nucleophilic attack was first investigated by use of conventional hydroxy-terminated PEO. As explained in a former paper, the PEO-reactant was exchanged with the dipentaerythritol-modified PEO, allowing the route toward the branched, star-shaped polymers (see Ref.[2]). In the latter case, the attacking alcoholate is hindered and shielded by the bulky dipentaerythritol, complicating the accessibility of the mesylated endgroup. In contrast, the primary alcoholate derived from mere PEO is more reactive. These assumptions were verified experimentally. Starting with commercially available PEO (after precipitation and drying), a considerable amount of diblock PEO-*b*-PPO is formed after one night under reflux (see Figure S 1). In case of the sterically hindered dipentaerythritol-derivative as alcoholate, the reaction time needs to be increased by more than 300 % and the amount of NaH was increased in order to obtain a similar result (see Ref.[2]). Traces of triblock copolymers were visible during Size Exclusion Chromatography (SEC) for the reaction of both dipentaerythritol-modified and unmodified PEO (forming a Pluronic™-type of Polymer). The reaction of unmodified PEO with bismesylated PPO was quenched with acetic acid. The excess of PPO was removed by crystallization of PEO in cold THF, leading to larger, precipitating aggregates, which consist mainly of diblock copolymers. The free PPO is well soluble in THF or hexane and can be decanted and discarded after centrifugation. Unexpectedly, SEC revealed that not all of the PEO was modified, as seen by the right-wing shoulder in the eluogram (see Figure S 1). These homo-PEO impurities can be removed by fractionated precipitation.[2] Thus, the nucleophilic attack on mesylated PPO is more difficult as compared to the well-know and

well-understood attack of nucleophiles on mesylated PEO (with its well accessible leaving group).[1, 3, 12]

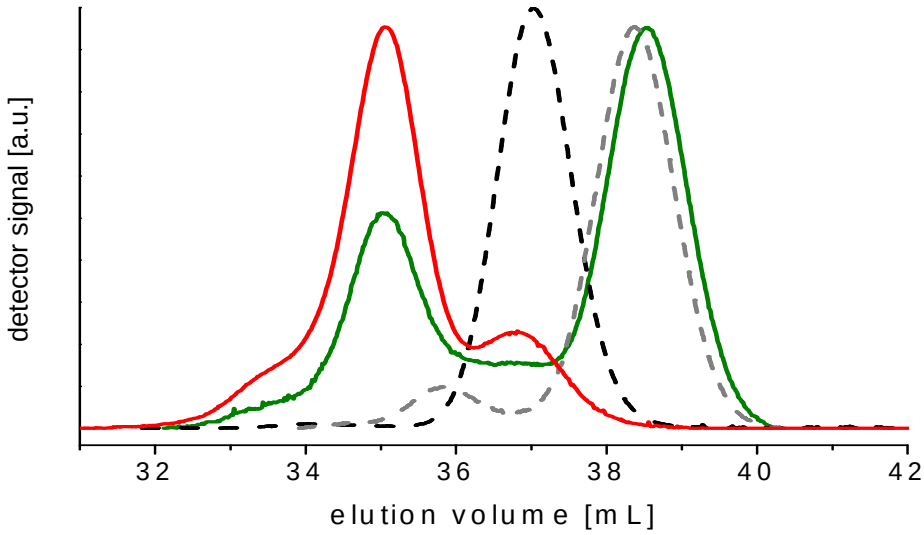

Figure S 1: RI-based eluograms obtained by size exclusion chromatography (SEC) of mesylated PPO_{69} (dashed gray) and PEO_{114} (dashed black) reactants, crude coupling product (green) and PEO_{114}-*b*-PPO_{69} diblock product (red) after partial purification

PPO-b-PDMAEMA Diblock Synthesis. For comparison, we also prepared diblock copolymers based on PPO and PDMAEMA. For this reason, we used commercially-available mono-alkylated PPO of average molecular weight M_n ~ 2500 g/mol (with rather broad distribution: $Đ_{M,SEC}$(PMMA-standards) = 1.4) for esterification with an ATRP initiator. ^{1}H NMR shows 61 % esterification under the assumption $M_n \approx$ 2500 g/mol (Figure S 2). However, the workup by dialysis apparently fractionated the sample, leaving pure macroinitiator of higher M_n inside the dialysis membrane. Thus, the molecular weight M_n can be calculated from the NMR, when assuming full esterification of the telechelic polymer ($M_n \approx$ 4000 g/mol, $DP_n \approx$ 69). This value is very much in line with the endgroup analysis of the combined integral over the butyl and allyl moieties, which comprise the other endgroup (allyl is made by transfer to monomer during anionic PO - polymerization). So, we obtained a

similar length of PPO on number average as compared to our miktoarm star. SEC of the PPO macroinitiator corroborated the presence of transfer to monomer during propylene oxide polymerization (see Figure S 3). Besides a shoulder at higher molecular weight (presumably due to coupling), a sharp peak (most likely butyl-terminated PPO) is accompanied with a low molecular weight shoulder (most likely allyl-terminated PPO). The fractionation is seen in the trace of the permeate after dialysis, which has a considerable smaller molecular weight.

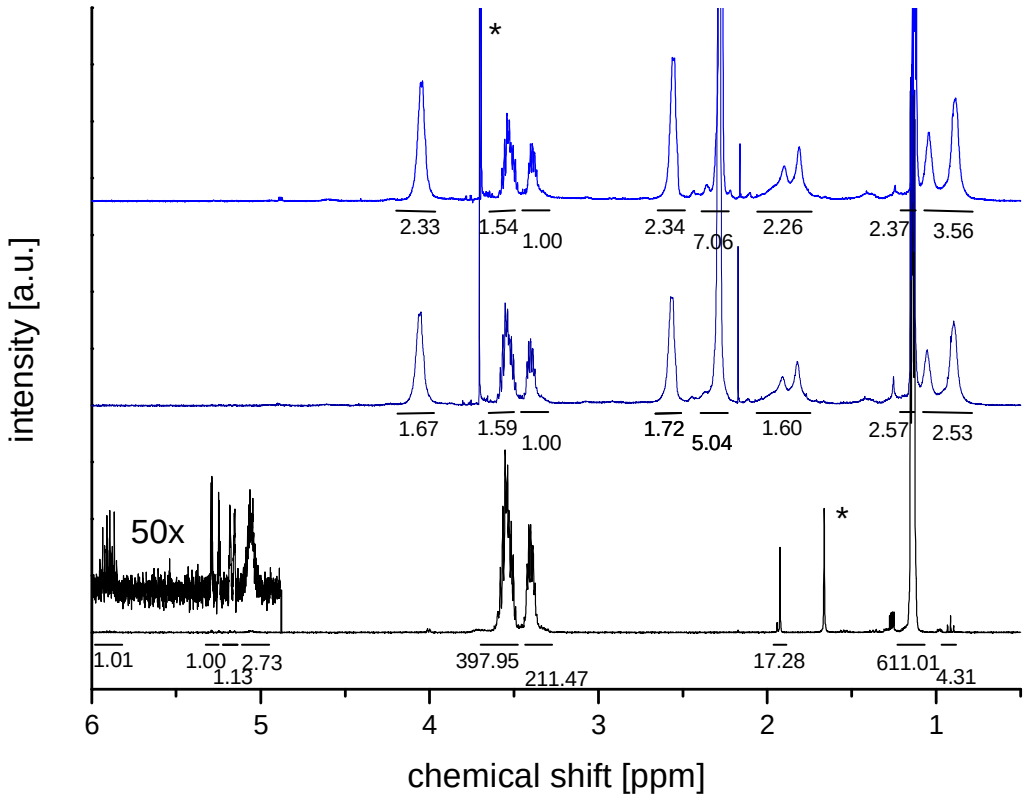

Figure S 2: ^{1}H NMR spectra in $CDCl_3$ of PPO_{69}-Br macroinitiator (black bottom curve; inset: enlarged area of allyl protons together with $–CH_2$-C(CH_3)*H*-O-proton adjacent to the ester bond), PPO_{69}-*b*-$PDMAEMA_{68}$ (dark blue spectrum in the center) and PPO_{69}-*b*-$PDMAEMA_{100}$ (blue top spectrum)

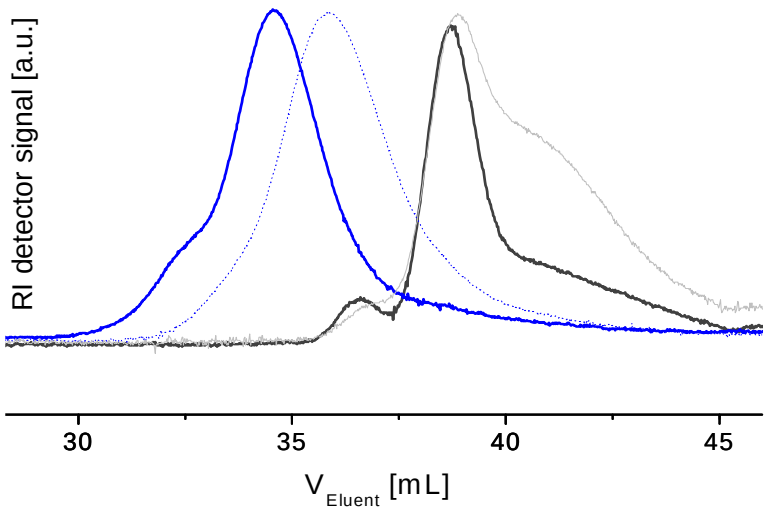

Figure S 3: RI-Traces obtained by size exclusion chromatography (SEC) of PPO_{69}-Br macroinitiator (dialysate, black curve), PPO-Br (permeate, grey curve), PPO_{69}-*b*-$PDMAEMA_{68}$ (dark blue, doted curve) and PPO_{69}-*b*-$PDMAEMA_{100}$ (blue curve)

During Atom Transfer Radical Polymerization (ATRP), one sample was drawn from the reaction mixture and the rest of the solution was allowed to continue its polymerization until 70% conversion after 4 h total reaction time. At intermediate conversions (48 %), the SEC eluogram becomes monomodal. At higher conversions (70 %), traces of coupling product due to recombination shows up as a shoulder at the high molecular side of the eluogram, which under certain circumstances could even partially originate from the coupled macroinitiator (Pluronic^{TM}-type of polymer). The molecular weight was determined by comparing the integrals of the PPO peaks with the integrals of the PDMAEMA peaks in NMR and assuming a DP_n(PPO)=69. The shorter polymer was assigned the formula $(PPO)_{69}$-*b*-$(PDMAEMA)_{68}$, whereas the larger diblock is best described with $(PPO)_{69}$-*b*-$(PDMAEMA)_{100}$. The characterization is summarized in Table S 1 and in Table 1 in the Main Part.

Table S 1: Molecular Characterization of the Prepared Diblock Copolymers

	time, conversion for ATRP	M_n(theo) [g/mol]	M_n(NMR) [g/mol]	M_n(SEC) [g/mol] ($Đ_{M,SEC}$)
PPO_{69}-*b*-$PDMAEMA_{68}$	1.75 h, 48 %[a]	15000[b]	15000[c]	10400 (1.35)[d]
PPO_{69}-*b*-$PDMAEMA_{100}$	3 h, 70 %[a]	20000[b]	20000[c]	21900 (1.10)[d]
PEO_{114}-*b*-PPO_{69}	-	9000[e]	9000[c]	16900 (1.10)[d]

[a] time and conversion as used for ATRP of DMAEMA; conversion measured by comparison of ^{1}H NMR signal of oxygen-connected methylene group of monomer and polymer at 4.2 or 4.05 ppm respectively
[b] calculated by molar ratio of monomer / initiation site times the conversion (as seen by ^{1}H-NMR); molar mass of the macroinitiator has been added
[c] calculated by ^{1}H NMR assuming a molar mass of the PEO moiety of 5000 g/mol (or 4000 g/mol for PPO block for PDMAEMA-based linear polymers)
[d] apparent molecular weight and dispersity ($Đ_M$) as determined by SEC in DMF and using PMMA standards
[e] sum of molecular weight of the precursors

Synthesis of Miktoarm Starpolymers: The synthesis is described in detail in a former publication.[2] The pathway toward the stars is highlighted in Scheme S1.

Scheme S1: Synthetic Strategy toward the Ternary Star Polymers (adapted from Ref.[2] with permission from The Royal Society of Chemistry)

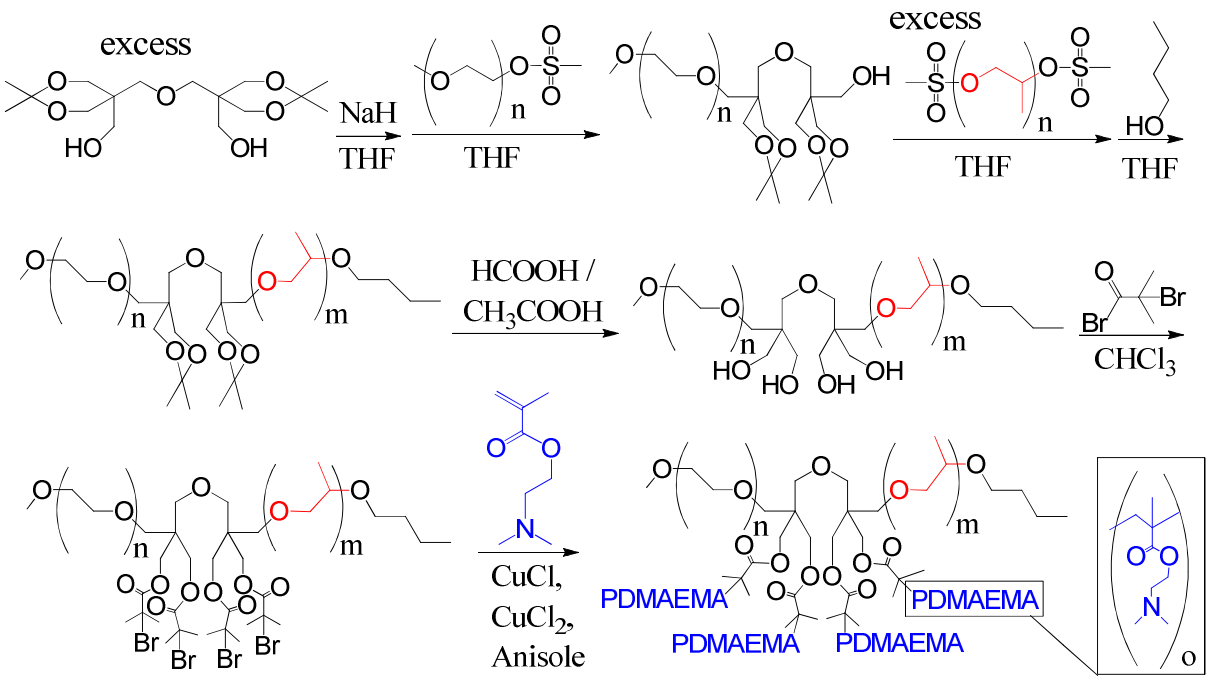

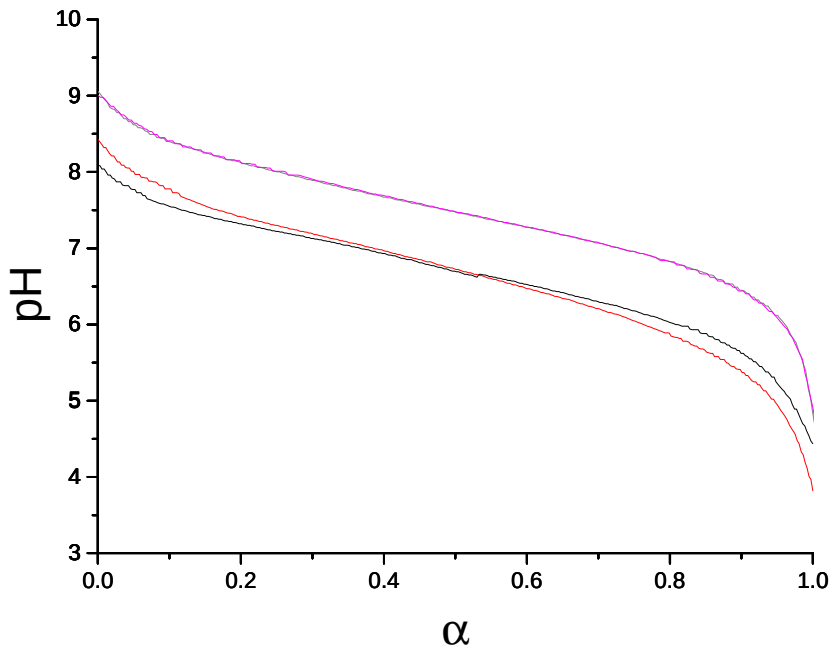

Figure S 4: comparison of titration curves (pH against degree of neutralization α) for PEO_{114}-$(PDMAEMA_{90})_{3.1}$-PPO_{69} (grey and black lines) and PEO_{114}-$(PDMAEMA_{110})_{2.5}$ (red and pink lines) in 0.1 M NaCl at 25 (grey and pink lines) and 60 °C (black and red lines).

Titration. The charging of PDMAEMA was followed by potentiometric titrations. We compared the ternary miktoarm star PEO_{114}-$(PDMAEMA_{90})_{3.1}$-PPO_{69} with the binary PEO_{114}-$(PDMAEMA_{110})_{2.5}$ (Figure S4). At low temperatures, both titration curves superimpose very much and effects of complexation are not reflected in the titration behavior. However at elevated temperatures, the titration curve for the star with possible PPO/PDMAEMA complexation is less steep. This might be a result of enhanced complexation between PPO and PDMAEMA, which is in line with fluorescence results (main part): less PDMAEMA units are accessible for hydroxide production at low degrees of neutralization, which lowers the pH. In addition, the results show that the PDMAEMA is almost uncharged at pH 8 at 60°C, while some residual charges remain at low temperature. It is known that increasing temperature leads to a decrease of charging of the PDMAEMA units.[13] This result indicates that the stabilization of the unimolecular micelles are not only driven by electrostatic repulsion between the PPO-based miktoarm stars, but interfacial effects and enhanced complexation with temperature play a crucial role, especially shortly before the phase transition of PDMAEMA (see Figure 8 in the main part: concentration of aggregates reduces even upon heating, which is opposite to the trends of electrostatic stabilization).

Fluorescence Spectroscopy for cmc-Determination. Pyrene is a prominent molecule for the determination of the critical micellization concentration (*cmc*).[14-16] As an assumption, the presence of hydrophobic domains attends the aggregation of the amphiphilic molecules. Obviously, this is not true for unimolecular micelles, which usually keep the hydrophobic compartments throughout the concentration regimes.[17] Generally, the *cmc*-determination of polymeric amphiphiles with help of fluorescence spectroscopy can be problematic, since long non-polar blocks will be hardly hydrated even in the very dilute regime and the hydrophobic character is still kept (e.g. the soluble block can wrap around the hydrophobic domain of possible unimers). More complicated, the solubilization equilibrium of the hydrophobic

fluorescent probe within the hydrophobic compartment can change upon lowering the polymer concentration. Then, the solubilization equilibrium turns in favor of free fluorescent dye in case of low polymer concentration, though non-solvated chains are still present in the system. Thus, the *cmc*-determination in case of our polymers is only of limited significance (Figure S 5) and is therefore better characterized as the minimum polymer concentration, at which the fluorescent probe can be detected in an unpolar environment. It appears that the pyrene starts to be solubilized by the hydrophobic compartments at polymer concentrations higher than approximately $4 \cdot 10^{-7}$ mol/L (which is rather similar to the pyrene concentration). This behavior is irrespective of the polymer used. Therefore, only the PPO concentration (which is approximately the same for all polymers) determines the onset of dye solubilization.

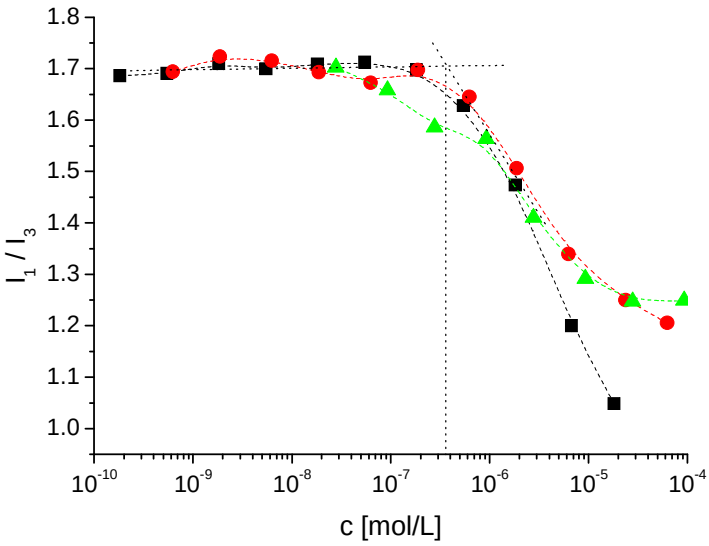

Figure S 5: comparison of the ratio of the vibronic bands I_1 and I_3 of aqueous solutions containing miktoarm star PEO_{114}-$(PDMAEMA_{90})_{3.1}$-PPO_{69} (black squares) or diblock copolymers (PEO_{114}-*b*-PPO_{69} – green triangles – and PPO_{69}-*b*-$PDMAEMA_{100}$ – red circles) by using the pyrene method ($c_{pyrene} = 5 \cdot 10^{-7}$ mol/L; solvent: pH8 buffer in 0.1 M NaCl; 20°C), as used for *cmc* - determinations.

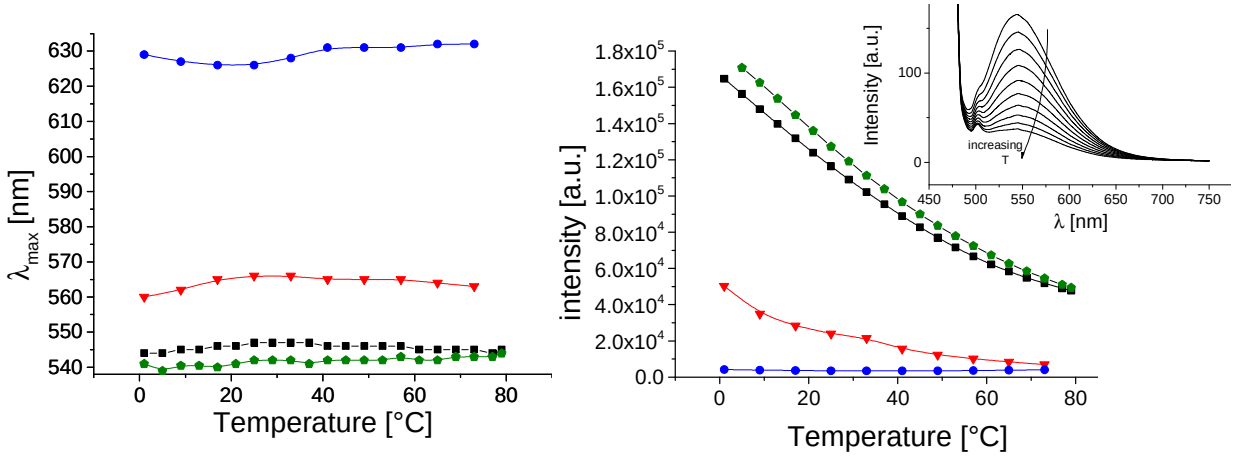

Figure S 6: Emission maximum λ_{max} (left) of pH8 buffer in 0.1 M NaCl (blue circles), PPO_{69} (red triangles), $PDMAEMA_{1200}$ (green pentagons) and PDMAEMA/PPO complex (black squares; prepared from 0.07 g PPO_{69} and 0.43g $PDMAEMA_{1200}$) by using the 4HP method (c_{4HP} = 1 · 10^{-6} mol/L; λ_{exit} = 470 nm, λ_{em} = 480−750 nm); right: integrated intensity of the emission band as depicted in the inset (here showing the behavior of the PDMAEMA/PPO complex).

4HP Fluorescence - Comparison of Dye in Brine, PPO and PDMAEMA. To relate the fluorescence signals of 4HP to its respective surroundings, the 4HP fluorescence was measured in pure brine, pure PPO, pure PDMAEMA and PPO/PDMAEMA complex with a mass ratio of 1:6. A mixture with similar mass ratio between the components was reported to be miscible.[11] As seen in Figure S6, the wavelength at the maximum in the emission spectra is lowest for the non-aqueous PDMAEMA-containing systems. At the same time, the fluorescence signal increases drastically for the complex and for mere PDMAEMA. This indicates a negligible influence of 4HP fluorescence quenching induced by tertiary amine groups as reported for pyrene.[18] The similarity of λ_{max} between non-aqueous PDMAEMA and non-aqueous PPO/PDMAEMA mixture indicates that the reason for the low λ_{max} is dominated by the presence of non-hydrated PDMAEMA (a synergistic depression of λ_{max} in case of the complex is not detected). Therefore, the 4HP results of PEO_{114}-$(PDMAEMA_{90})_{3.1}$-PPO_{69} are

in line with a PDMAEMA-rich, sparely hydrated domain even in diluted aqueous solution when comparing to the 4HP response of a PEO_{114}-$(PDMAEMA_{110})_{2.5}$ solution (see the main part). For the latter case, PDMAEMA is well hydrated below its cloud point and probably even partly above its cloud point. Then, differences in the 4HP response between PEO_{114}-$(PDMAEMA_{90})_{3.1}$-PPO_{69} on one side and the diblock copolymers on the other side are either due to a different partitioning of the dye between these non-aqueous domains and/or a changed λ_{max} for the PDMAEMA-rich, hydrophobic domain (compared to a PPO domain). In both cases, a special interaction between PPO and PDMAEMA is required in order to explain the 4HP results obtained from PEO_{114}-$(PDMAEMA_{90})_{3.1}$-PPO_{69}.

Pyrene Fluorescence. A similar procedure as shown in Figure S6 was also tried for pyrene, which has its excitation in the UV. Probably due to some fluorescent impurities (e.g. from the azobisisobutyronitrile initiator used for PDMAEMA polymerization), a straightforward evaluation of the pyrene data at that high PDMAEMA concentration was not possible (overlap of fluorescence signals). But it is reasonable to assume that the pyrene experiences a similar low polarity for pure, non-aqueous PDMAEMA as was detected for 4HP. By complexation, the reduced polarity of a PDMAEMA-rich, sparely-hydrated phase is transferred to the diluted aqueous phase, which explains the lower I_1/I_3 ratio in case of the miktoarm star compared to the higher I_1/I_3 ratio for pyrene in pure PPO (at low temperature; see main part).

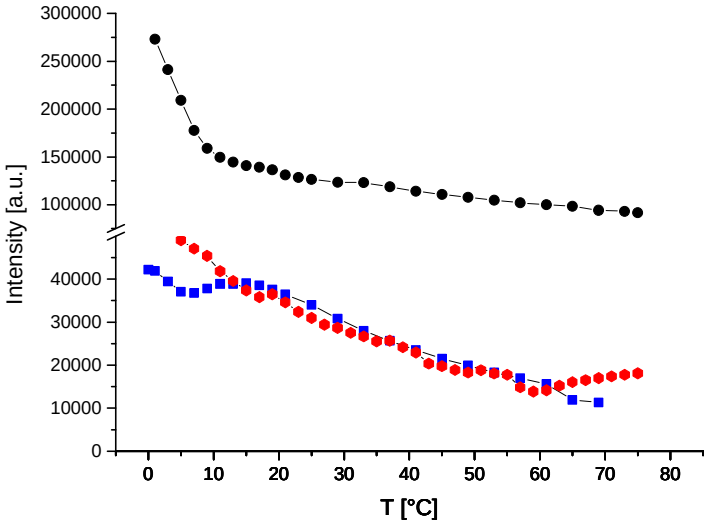

Figure S 7: Fluorescence intensity of pyrene ($5 \cdot 10^{-7}$ M pyrene; λ_{exit} = 333 nm, λ_{em} = 340 - 500 nm) in pH 8 buffer (+ 0.1 M NaCl) containing 0.4 g/L PPO_{69}-*b*-$PDMAEMA_{100}$ (blue squares), 0.16 g/L PEO_{114}-*b*-PPO_{69} (black circles) or PEO_{114}-$(PDMAEMA_{90})_{3.1}$-PPO_{69} (red hexagons)

To check the influence of pyrene quenching induced by tertiary amines, the integrated fluorescence intensities of pyrene are measured for the three polymers (Figure S7). The presence of PDMAEMA in the PPO-based copolymers induces a drop in intensity, indicating a pronounced, but not drastic fluorescence quenching.

Therefore, fluorescence spectroscopy was performed with pyrene as a probe also for PPO_{69}-*b*-$PDMAEMA_{100}$ (Figure S8). In comparison to the result obtained with 4HP (see Main Part), pyrene shows a more hydrophobic scenario. Within the accessible temperature region, the I_1/I_3 ratio of the pyrene emission does not go to the fully hydrated case even for low temperatures. In addition, the curve is always below the curve obtained for PEO_{114}-*b*-PPO_{69}. Comparing to the results obtained with pyrene and PEO_{114}-$(PDMAEMA_{90})_{3.1}$-PPO_{69} (e.g. lower I_1/I_3 ratio than in pure PPO at low temperature), pyrene seems to sense a more hydrophobic environment in presence of both PDMAEMA and PPO than 4HP. Still, there is a

strong increase in the I_1/I_3 ratio below 8 °C, which indicates some hydration of the PPO at low temperatures.

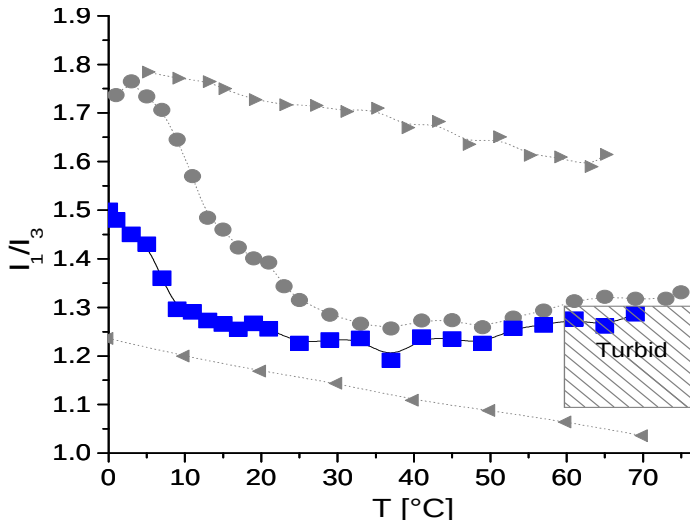

Figure S 8: Fluorescence spectroscopy of pyrene (intensity ratio of the first – λ_{em} = 373 nm – and third vibronic fluorescence band – λ_{em} = 383 nm; 5 · 10^{-7} M pyrene; λ_{exit} = 333 nm, λ_{em} = 340 - 500 nm) in pH 8 buffer (+ 0.1 M NaCl) containing 0.4 g/L PPO_{69}-*b*-$PDMAEMA_{100}$ (blue squares), 0.16 g/L PEO_{114}-*b*-PPO_{69} (for comparison, taken from Main Part; gray circles) or no polymer (for comparison, taken from Main Part; gray triangles; directed toward the right: pyrene in pure aqueous solvent; directed toward the left: pyrene in pure PPO 4000); part of data reprinted with permission from *ACS Macro Lett.*, 2012, **1**, 504. Copyright 2012 American Chemical Society.

Part of the differences between the spectroscopic results of pyrene and 4HP can be explained by the quenching of pyrenes in the vicinity of tertiary amines. At the same time, the resulting signal might be dominated by the pyrene molecules remote from the amines (e.g. the ones in the pure PPO domain). However, the smaller I_1/I_3 values for pyrene in presence of PEO_{114}-$(PDMAEMA_{90})_{3.1}$-PPO_{69} compared to pyrene in pure PPO indicate that the quenching alone is not the mere reason for low I_1/I_3 values (see main part). Otherwise similar I_1/I_3 values

for pyrene in pure PPO should have been obtained also for PEO_{114}-$(PDMAEMA_{90})_{3.1}$-PPO_{69} as a limiting scenario (when assuming the absence of complexation). Hence, complexation between PPO and PDMAEMA in the star might explain this behavior (leading to a different partitioning of pyrene and/or different I_1/I_3 values for the complex domain). Still, the obtained results allow the assumption of a preferred location of pyrene, which is somewhat different compared to the one of 4HP. Comparing the 4HP data with the pyrene data, the I_1/I_3 values for PPO_{69}-*b*-$PDMAEMA_{100}$ and PPO_{69}-*b*-PEO_{114} are not as superimposing at higher temperatures as those for λ_{max} (see main part). Probably, the 4HP is well incorporated in the PPO-domain, while pyrene might still feel also the presence of PDMAEMA (maybe sitting more at the interface). Interestingly, the intensity increases again after collapse of PPO for PPO_{69}-*b*-$PDMAEMA_{100}$ toward the behavior of PEO_{114}-$(PDMAEMA_{90})_{3.1}$-PPO_{69} (Figure S 7). This might be in line with the fact that the pyrene has an increased contact to PPO after PPO collapse.

Summarizing, the pyrene method is still suitable for the investigation of the used polymers, though 4HP has some advantages (like increased fluorescence signal in presence of polymer due to increased microviscosity, negligible fluorescence quenching induced by the polymers, clarity of spectral changes including the fluorescence intensity upon phase transitions, dual responsivity to microviscosity and polarity).

PPO Solubility. The PPO solubility in water and its thermoresponsive behavior were investigated by turbidity and fluorescence spectroscopy of an aqueous solution of the same PPO precursor, which was used for the preparation of the miktoarm stars (using 4HP as dye; see Figure S 9). It can be seen that the PPO turns hydrophobic before the PPO chains start to aggregate and precipitate. The polarity indicator λ_{max} starts to decrease at about 5 °C, indicating the presence of hydrophobic domains long before macroscopic phase separation

takes place (at around 13°C). The microviscosity indicator (total intensity) goes then very much in line with the macroscopic phase separation, implying the presence of a partially hydrated PPO chain with small hydrophobic domains (maybe even as a pearl-necklace-type of structure), where the microviscosity within the domains is not much changed yet.

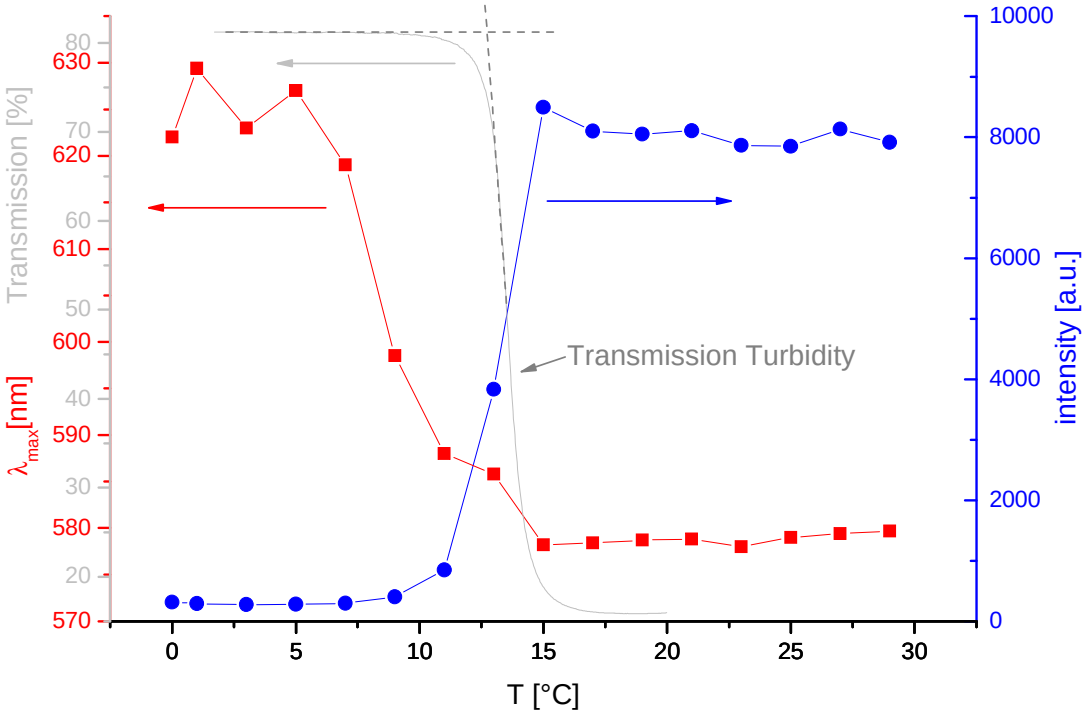

Figure S 9: Comparison of the fluorescence (wavelength at the maximum in the emission spectrum λ_{max} – in red squares – and total fluorescence intensity – in blue circles) and the turbidity data (black full curve; at 600 nm) of a PPO_{69} solution in pH 8 buffer (0.1 M NaCl; 0.05 wt.% PPO; M_n(PPO) = 4000 g/mol; heating rate 20 K/h; 0.002 g/L 4HP, λ_{ex} = 470 nm, λ_{em} = 480 - 750 nm); part of data reprinted with permission from *ACS Macro Lett.*, 2012, **1**, 504. Copyright 2012 American Chemical Society.

NMR-Spectroscopy. In order to gain further information on the complexation, ^{1}H 2D NMR NOESY spectra were recorded both for the miktoarm star and the diblock in aqueous solution (Figure S11).[6] Whereas cross peaks and therefore the special interaction between PPO and

PDMAEMA are clearly seen in the case of the miktoarm star,[6] there is hardly any evidence for such cross peaks in the case of the diblock copolymer. In both cases, the spectra were taken at 23 °C, where predominantly micellar structures (either unimolecular or intermolecular aggregation) are expected according to the light scattering results (see Main Part). In addition, the PPO methyl signal at 1.1 ppm has shifted upfield compared to the signal at roughly 1.2 ppm in case of the miktoarm star and generally in case of PPO samples in chloroform.[6] It overlaps quite strongly with the PDMAEMA backbone methyl group signals. This shift is an indication that the surroundings of PPO in the diblock are different compared to the miktoarm star, which is reasonable when assuming a PPO-core star-shaped micelle. In addition, there are strong cross peaks between the PPO backbone protons and the PPO methyl protons (marked by a purple circle), which indicates additional proximity between these groups. The miktoarm star has weaker internal PPO cross signals (in blue), but there are clear PPO / PDMAEMA cross peaks (in red), which is well in line with the complexation within the star. Besides the interaction with the dimethylamino group (at 2.5 ppm), the PPO backbone protons (at 3.6 – 3.2 ppm) seem to interact predominantly with certain microstructures of the PDMAEMA backbone, since there are no crosspeaks with the (*rr*) PDMAEMA backbone methyl proton signals at 0.9 ppm (but only with the backbone methyl proton signals at 1.0 ppm). This can be understood with the sterical requirements of interaction (e.g. *mr* PDMAEMA triads could offer pockets of the right dimensions for the insertion of the PPO backbone, while *mm* and *rr* triads are less effective). All in all, this NMR experiment (Figure S11) corroborates again the special interaction of PDMAEMA and PPO within the miktoarm star.

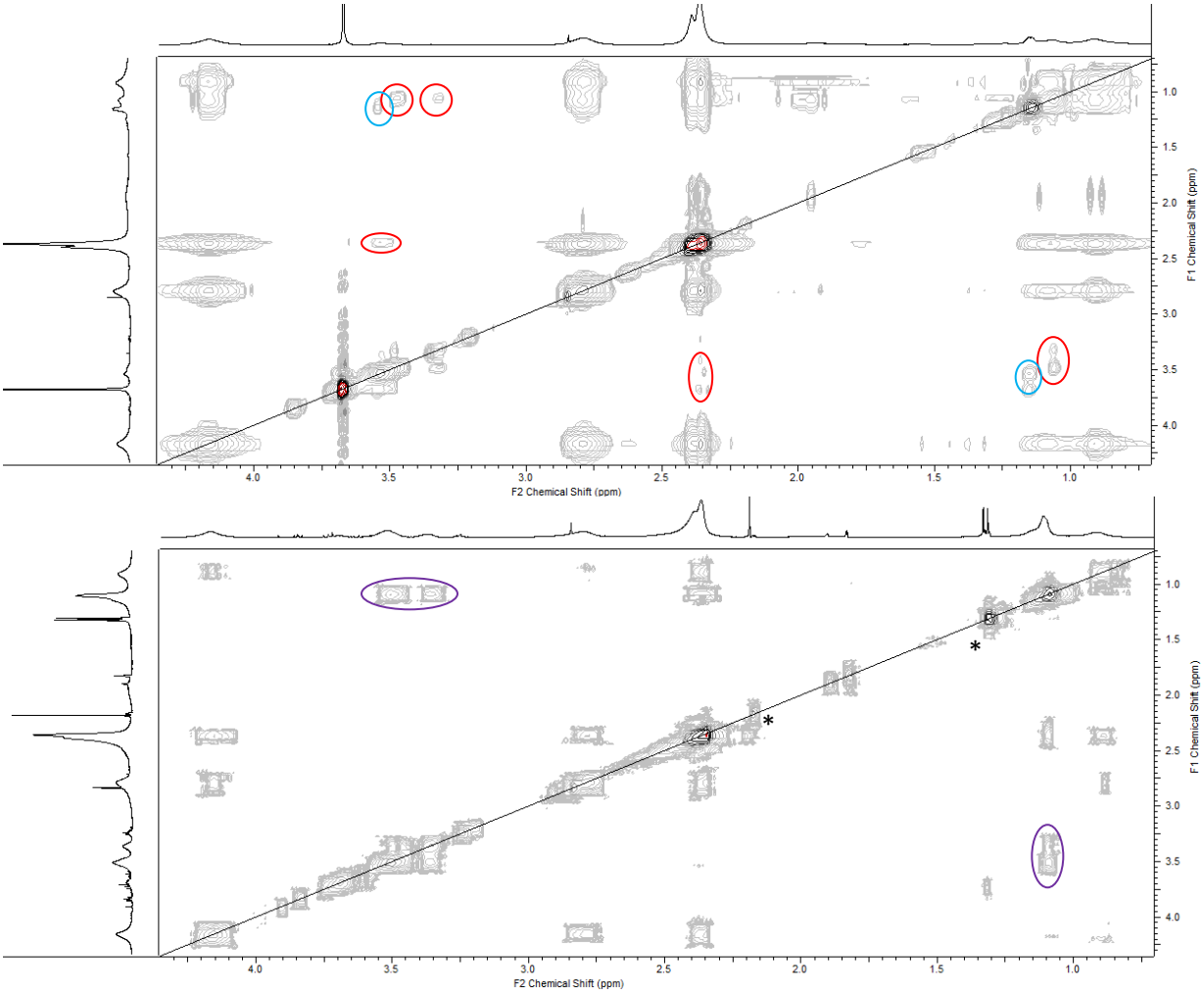

Figure S11: ^{1}H 2D NMR NOESY spectra of PEO_{114}-$(PDMAEMA_{90})_{3.1}$-PPO_{69} (~ 10 mg/mL, top) and PPO_{69}-b-$PDMAEMA_{100}$ (~ 4 mg/mL, bottom) in D_2O (containing pH 8 buffer and 0.1 M NaCl) taken at 23 °C; red circles assign clear PPO / PDMAEMA crosspeaks; blue circles assign internal PPO cross signals; purple circles most likely assign PPO cross peaks; asterisk indicates solvent impurities; top spectrum taken from Ref.[6] (part of data reprinted with permission from *ACS Macro Lett.*, 2012, **1**, 504. Copyright 2012 American Chemical Society).

Hysteresis as detected by Light Scattering: We also investigated shortly the extent of hysteresis within one heating and cooling circle (Figure S12). A simple light scattering experiment revealed pronounced hysteresis for the diblock copolymer PEO_{114}-*b*-PPO_{69} (here probably due to the loose aggregates), but only minimal hysteresis for PEO_{114}-$(PDMAEMA_{90})_{3.1}$-PPO_{69}. Apparently, the aggregates based on insoluble PDMAEMA disassemble more easily than the ones based on PPO-core micelles. The high water content in the PDMAEMA-rich domains might be the reason for this behavior.

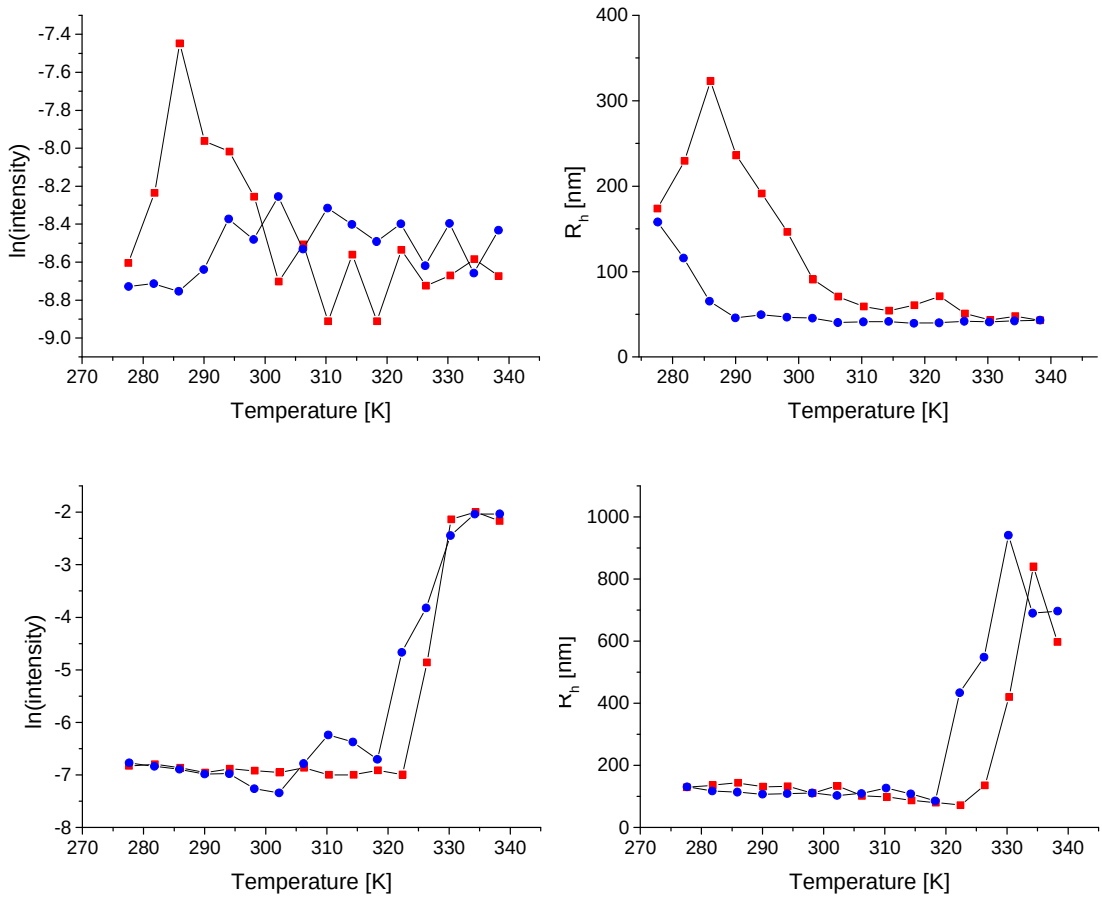

Figure S12: Manifestation of hysteresis during heating (red) and subsequent cooling (blue): right: average hydrodynamic radius obtained by second order cumulant analysis at an angle of 30°; left: logarithm of the scattering intensity at an angle of 30°; top: PEO_{114}-*b*-PPO_{69}, bottom: PEO_{114}-$(PDMAEMA_{90})_{3.1}$-PPO_{69}

Small Angle X-ray Scattering (SAXS): For further comparison, we measured SAXS of a PEO_{114}-*b*-PPO_{69} solution at low and high temperatures. In order to gain an acceptable signal to noise ratio, we needed to increase the concentration to 3 g/L (Figure S13). After subtraction of scattering signal of the micellar solution with a unimer solution, the data could be modeled with a micellar form factor.[19] The obtained parameters are consistent with former investigations on similar systems.[20, 21] The aggregation number N_{agg} is in the range of 200, which is about 10 times larger than the values obtained by fluorescence quenching experiments (see Ref.[6]; this discrepancy can be easily explained by the 6 times larger hydrophobic core volume compared to the Förster volume;[22] in case of unimolecular micelles, the Förster volume is larger than the hydrophobic domain size and N_{agg} obtained by fluorescence quenching is a realistic one).[6] The radius of gyration for the whole micelle was determined as 16 nm (R_g / R_h ≈ 0.8, which is close to a compact structure in case of homogenous scattering contrast).

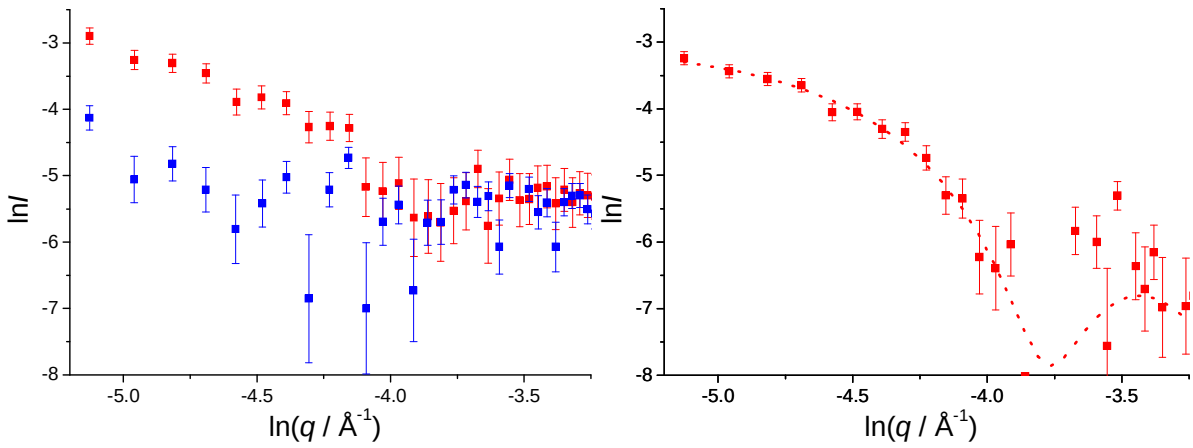

Figure S13: Small angle X-ray scattering data (SAXS) of a 3 g/L PEO_{114}-*b*-PPO_{69} solution in pH 8 buffer and 0.1 M NaCl at 3°C (blue) and at 45°C (red; both left hand side) and the subtracted data to resolve the micellar form factor (right hand side; dotted red line: modeled form factor according to polymeric micelle form factor model with Gaussian distribution in core size: R_{core} = 7±1 nm; n_{agg} = 0.35 chains/nm^2; aggregation number N_{agg} = 210; radius of gyration for a corona chain $R_{g,CoronaChain}$ = 4.5 nm; chain volume in corona $V_{CoronaChain}$ = 4 nm^3; contrast electron densities: $\eta_{core} = 3.2 \cdot 10^{-8}$ Å^{-3}; $\eta_{brush} = 3.2 \cdot 10^{-7}$ Å^{-3}; $\eta_{solvent} = 4.9 \cdot 10^{-8}$ Å^{-3}; last values should be only taken relatively, since scattering data was not normalized to concentration)

Further, we measured also SAXS of the miktoarm star solution, though we could not access a broader scattering range. Thus only the Guinier regimes were recorded (Figure S14). Here, the scattering profile does not change significantly with temperature. A Guinier-plot at 20 °C revealed the radius of gyration R_g of the unimolecular micelles (R_g ~ 5 nm). Thus, R_g / R_h is close to unity, though higher values are expected for stars with rather low arm numbers (R_g / R_h around 1.5 for stars with 6 polydisperse arms).[23] However, the observed R_g / R_h is in between the limits for stars and compact spheres (R_g / R_h ~ 0.78). Therefore, this data corroborates again the internal compartmentalization, which leads to a concentration of

polymer at the center of the star. In addition, R_g of the spherical, star-shaped micelles, which are comprised of stars, could be also extracted as well (R_g ~ 24 nm). Thus, R_g / R_h is close to 1.5, which is a rather high number for spherical micelles (compare R_g / R_h in e.g. Ref.[21]) Again, it can be explained by a rather low aggregation number and possibly by increased contrast of the PDMAEMA corona (R_g / R_h around 1.5 for star-shaped micelles with 6 polydisperse "units").[23] Please note that the ratio of the extrapolated intensities I_0 for the miktoarm star unimers and miktoarm star micelles observed by the DLS/SLS approach and by the SAXS measurements coincide well. This is another indication that the decomposing light scattering treatment works well and gives reasonable results.

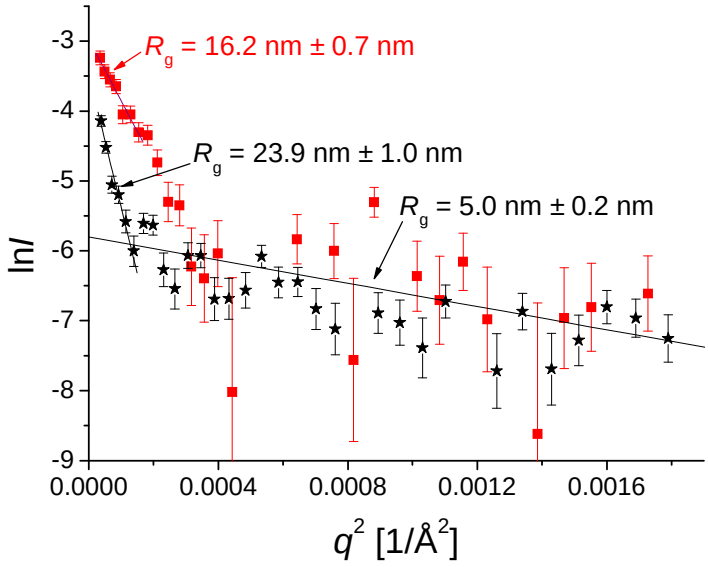

Figure S14: Guinier plot (obtained by SAXS) of a 1 g/L PEO_{114}-$(PDMAEMA_{90})_{3.1}$-PPO_{69} solution (at 20°C; black stars; raw data was background corrected by subtraction of solvent scattering) and 3 g/L PEO_{114}-*b*-PPO_{69} solution (at 45 °C; red squares; raw data was background corrected by subtraction of sample scattering at 3°C) in pH 8 buffer and 0.1 M NaCl for extraction of radius of gyration R_g

Cryo SEM of Multimolecular Micelles of Miktoarm Stars (Elevated Temperature): Scanning Electron Microscopy of vitrified samples (cryo-SEM) gave further evidence of spherical polymer aggregates in the size range of 1-7 µm after partial sublimation of water (see Figure S15). During sublimation, also salt crystals are formed (e.g. seen as hexagonal structures), which originate from the buffered solution.

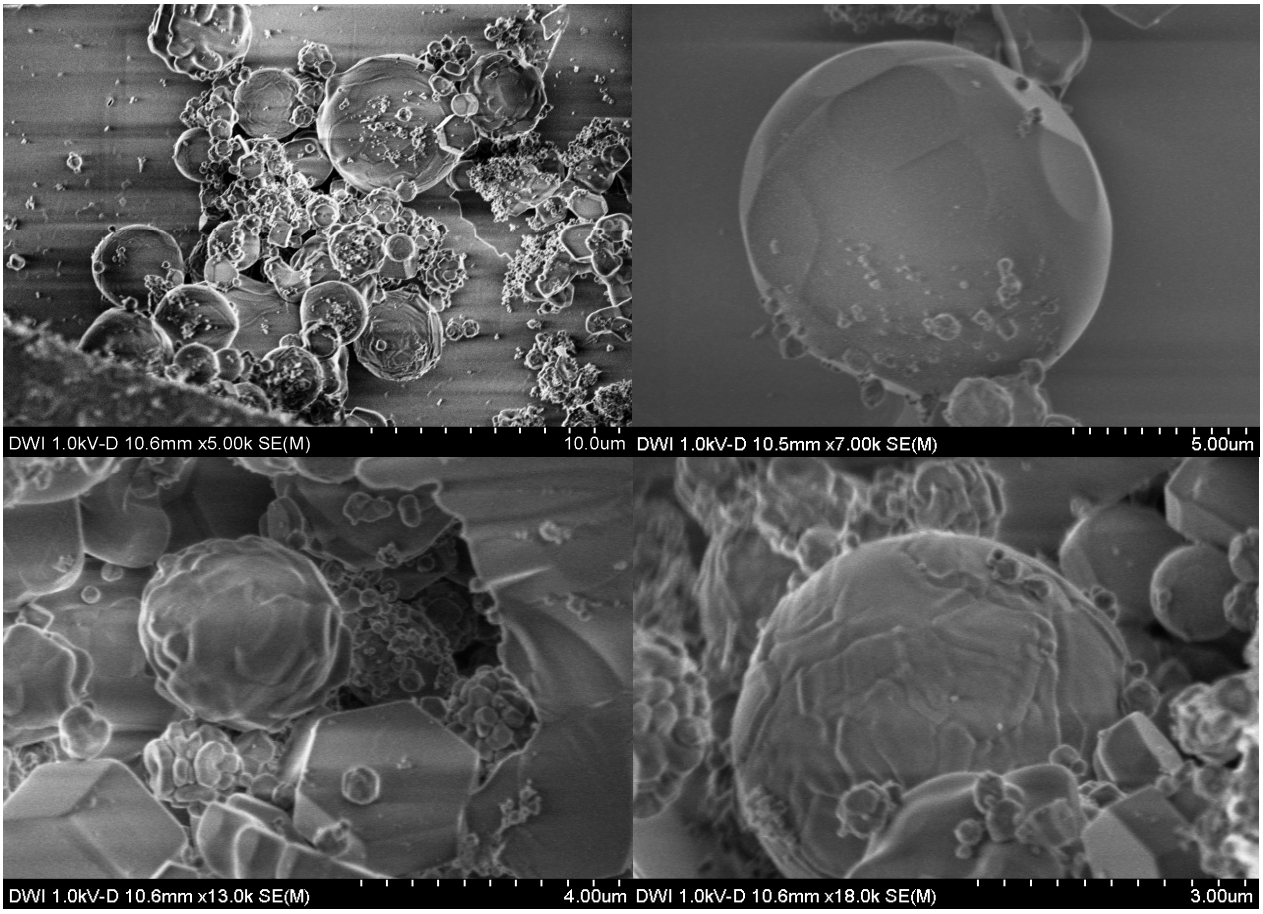

Figure S15: Cryo-SEM images of 1g/L solution of PEO_{114}-$(PDMAEMA_{90})_{3.1}$-PPO_{69} (in pH 8 buffer and 0.1 M NaCl) kept at 70°C over night and vitrified from approximately 70°C (scale bares of 10, 5, 4 and 3 µm total size are subdivided into 10 parts as indicated by the white lines).

Cryo-STEM image of loose aggregates (room temperature): By use of cryo-STEM, both micellar structures and larger aggregates of the miktoarm stars could be detected, which is

well in line with the light scattering results (Figure S16). However, the prevalent unimolecular micelles could not be resolved by electron microscopy due to their small size, though they comprise the majority of the polymer in the system. Regarding the loose aggregates, their origin is still subject of controversy also for other systems.[24] E.g. "Nanobubbles"[25] can be discussed as a possible reason for the slow modes in DLS. However, the strong contrast of the larger aggregates seen in cryo-STEM suggests a different conclusion. Additionally, we performed DLS measurements of PEO_{114}-*b*-PPO_{69} after degassing by applying vacuum for 15 min (not shown). However, the DLS results did not change, implying that aggregation is the main reason for the slow modes rather than gaseous inclusions.

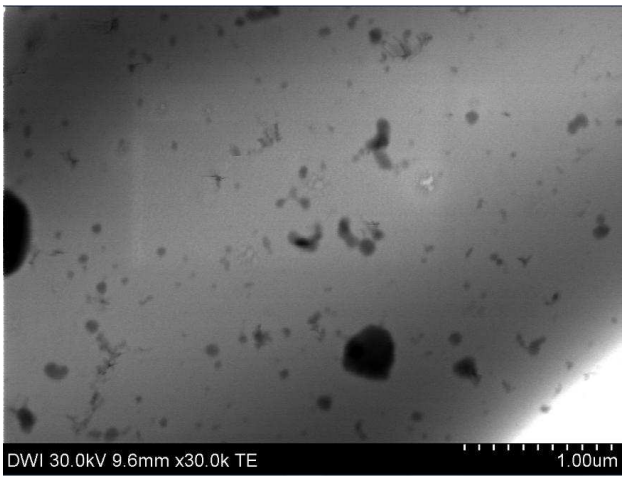

Figure S16: cryo-STEM image of a 1g/L solution of PEO_{114}-$(PDMAEMA_{90})_{3.1}$-PPO_{69} in pH 8 buffer and 0.1 M NaCl; sample was vitrified from room temperature (solution was filtered – 0.45 µm – prior TEM preparation)

REFERENCES

1 F. A. Plamper, J. R. McKee, A. Laukkanen, A. Nykänen, A. Walther, J. Ruokolainen, V. Aseyev and H. Tenhu, *Soft Matter*, 2009, **5**, 1812-1821.
2 A. Steinschulte, B. Schulte, N. Drude, M. Erberich, C. Herbert, J. Okuda, M. Möller and F. Plamper, *Polymer Chemistry*, 2013, **4**, 3885 - 3895.
3 F. A. Plamper, L. Murtomäki, A. Walther, K. Kontturi and H. Tenhu, *Macromolecules*, 2009, **42**, 7254-7257.
4 M. Save, J. V. M. Weaver, S. P. Armes and P. McKenna, *Macromolecules*, 2002, **35**, 1152-1159.

5 W.-S. Tan, Z.-C. Zhu, S. A. Sukhishvili, M. F. Rubner and R. E. Cohen, *Macromolecules*, 2011, **44**, 7767-7774.
6 A. A. Steinschulte, B. Schulte, M. Erberich, O. V. Borisov and F. A. Plamper, *ACS Macro Lett.*, 2012, **1**, 504-507.
7 R. Klucker, J. P. Munch and F. Schosseler, *Macromolecules*, 1997, **30**, 3839-3848.
8 E. Tarassova, V. Aseyev, A. Filippov and H. Tenhu, *Polymer*, 2007, **48**, 4503-4510.
9 A. J. F. Siegert, *MIT Rad Lab Rep No 465*, 1943.
10 M. Daoud and J. P. Cotton, *Journal de Physique*, 1982, **43**, 531-538.
11 A. Vesterinen, S. Lipponen, J. Rich and J. Seppälä, *eXPRESS Polym. Lett.*, 2011, **5**, 754-765.
12 F. A. Plamper, S. Reinicke, M. Elomaa, H. Schmalz and H. Tenhu, *Macromolecules*, 2010, **43**, 2190-2203.
13 F. A. Plamper, M. Ruppel, A. Schmalz, O. Borisov, M. Ballauff and A. H. E. Müller, *Macromolecules*, 2007, **40**, 8361-8366.
14 G. Marinov, B. Michels and R. Zana, *Langmuir*, 1998, **14**, 2639-2644.
15 K. Kalyanasundaram and J. K. Thomas, *J. Am. Chem. Soc.*, 1977, **99**, 2039-2044.
16 O. Colombani, M. Ruppel, F. Schubert, H. Zettl, D. V. Pergushov and A. H. E. Müller, *Macromolecules*, 2007, **40**, 4338-4350.
17 A. Laschewsky, *Adv. Polym. Sci.*, 1995, **124**, 1-86.
18 Y. Diaz-Fernandez, F. Foti, C. Mangano, P. Pallavicini, S. Patroni, A. Perez-Gramatges and S. Rodriguez-Calvo, *Chem. - Eur. J.*, 2006, **12**, 921-930.
19 J. S. Pedersen and M. C. Gerstenberg, *Macromolecules*, 1996, **29**, 1363-1365.
20 S. Manet, A. Lecchi, M. Imperor-Clerc, V. Zholobenko, D. Durand, C. L. P. Oliveira, J. S. Pedersen, I. Grillo, F. Meneau and C. Rochas, *J. Phys. Chem. B*, 2011, **115**, 11318-11329.
21 O. Colombani, M. Ruppel, M. Burkhardt, M. Drechsler, M. Schumacher, M. Gradzielski, R. Schweins and A. H. E. Müller, *Macromolecules*, 2007, **40**, 4351-4362.
22 P. Wu and L. Brand, *Anal. Biochem.*, 1994, **218**, 1-13.
23 W. Burchard, M. Schmidt and W. H. Stockmayer, *Macromolecules*, 1980, **13**, 1265-1272.
24 J. Yan, W. Ji, E. Chen, Z. Li and D. Liang, *Macromolecules*, 2008, **41**, 4908-4913.
25 P. Attard, M. P. Moody and J. W. G. Tyrrell, *Physica A*, 2002, **314**, 696-705.